9820 *Biochemistry* **2010,** *49,* 9820–9829
DOI: 10.1021/bi101136d

BIOCHEMISTRY
including biophysical chemistry & molecular biology
Article

Effect of Temperature on the Self-Assembly of the *Escherichia coli* ClpA Molecular Chaperone[†]

P. Keith Veronese and Aaron L. Lucius*

Department of Chemistry, The University of Alabama at Birmingham, 1530 3^RD Avenue South, Birmingham, Alabama 35294-1240, United States

Received July 16, 2010; Revised Manuscript Received August 30, 2010

ABSTRACT: Protein quality control pathways rely upon ATP-dependent proteases, such as *Escherichia coli* ClpAP, to perform maintenance roles in the cytoplasm of the cell. ATP-dependent proteases remove misfolded and partially synthesized proteins. This action is particularly important in situations where an unregulated accumulation of such proteins will have a deleterious effect on the cell. ClpAP is composed of a tetradecameric serine protease, ClpP (21.6 kDa monomer), and the ATPase/protein unfoldase ClpA (84.2 kDa monomer). ClpA also uses its protein unfolding activity to remodel proteins and protein complexes; thus, in the absence of the proteolytic component, ClpA is considered a molecular chaperone. Previous reports, by others, suggested that ClpA exists in a monomer−dimer equilibrium at 4 °C. In contrast, using a combination of sedimentation velocity, sedimentation equilibrium, and dynamic light scattering, we recently reported that ClpA exists in a monomer−tetramer equilibrium at 25 °C. Here we report an investigation of the effect of temperature on the self-association of the *E. coli* ClpA protein unfoldase using analytical ultracentrifugation techniques. The results of sedimentation velocity and sedimentation equilibrium experiments performed at multiple loading concentrations of ClpA over a range of temperatures from 3.9 to 38.2 °C are discussed. Sedimentation velocity experiments show a decrease in weight average $s_{20,w}$ at the extremes of temperature. This result, along with extensive sedimentation equilibrium data and analysis, suggests the presence of a dimeric intermediate of ClpA that is differentially populated as a function of temperature. Further, analysis of sedimentation equilibrium data as a function of temperature led us to propose a monomer−dimer−tetramer equilibrium to describe the temperature dependence of ClpA self-assembly in the absence of nucleotide.

ATP-dependent proteases are responsible for the removal of properly folded proteins as a means of cell cycle regulation and homeostasis in all organisms (*1*). ATP-dependent proteases, in both eukaryotes and prokaryotes, are critical components of protein quality control pathways, as they are necessary for the removal of damaged or misfolded proteins that can occur during heat shock or stress (*2*−*4*). *Escherichia coli* ClpAP, akin to other energy-dependent proteases, is constructed from two distinct enzymes, a protein unfoldase, ClpA, and a protease, ClpP (*5*, *6*). The hexameric ClpA protein couples the energy derived from ATP binding and hydrolysis to protein unfolding and polypeptide translocation. When associated with the tetradecameric ClpP, ClpA feeds the newly unfolded polypeptide chain into the central cavity of the ClpP oligomer, which contains the serine protease active sites sequestered from solution. Interestingly, ClpA can use this protein unfolding activity in the absence of ClpP to disassemble protein oligomers and is therefore defined as a molecular chaperone (*7*−*9*).

ClpA, from sequence analysis, belongs to the ATPases associated with various cellular activities (AAA+) family of proteins (*10*). AAA+ proteins make up a large superfamily of proteins that include a number of molecular chaperones, some DNA helicases, and cellular cargo transporters (*11*). These AAA+ proteins are defined by a number of conserved regions, including the canonical Walker A and Walker B motifs that make up the ATP binding and hydrolysis site, often termed a AAA cassette (*12*).

ClpA contains two of the AAA cassettes per monomer and therefore contains two ATP binding and hydrolysis sites per monomer (*13*). Current data suggest ClpA requires nucleoside triphosphate binding but not hydrolysis to assemble into the hexameric form that can associate with ClpP and thus form an active ATP-dependent protease (*14*). In addition, data suggest that one of the nucleotide binding sites is required for nucleotide-driven assembly (*15*).

ClpA requires nucleoside triphosphate binding to assemble into an oligomeric form that will bind to target sequences in protein substrates (*16*, *17*). Despite this, the relative affinities for nucleotide binding and any cooperativity between the two sites in ClpA are not known. To quantitatively examine the energetics of nucleotide binding, nucleotide-driven hexamer formation, and subsequent protein substrate binding in an accurate thermodynamic model for self-association of ClpA in the absence of nucleotide binding is required (*18*). Moreover, the model for self-association of ClpA must be determined under the same conditions (i.e., temperature, salt concentration and type, pH, etc.) as the model determined for nucleotide-driven self-association and subsequent binding to polypepetide substrates. Despite this,

[†]This work was supported by National Science Foundation Grant MCB-0843746 to A.L.L.

*To whom correspondence should be addressed: Department of Chemistry, The University of Alabama at Birmingham, 1530 3^RD Ave. S., Birmingham, AL 35294-1240. Phone: (205) 934-8096. Fax: (205) 934-2543. E-mail: allucius@uab.edu.

 Published on Web 10/05/2010

it has been concluded that ClpA resides in a mixture of monomers and dimers under all conditions on the basis of an examination of the self-assembly reaction at 4 °C (*19*).

We recently reported a thorough examination of the self-association properties of ClpA using sedimentation velocity, sedimentation equilibrium, and dynamic light scattering techniques at 25 °C. These results show ClpA exists as a mixture of monomers and tetramers at thermodynamic equilibrium and 25 °C (*19*). Maurizi and co-workers performed sedimentation equilibrium experiments and concluded that ClpA resides in a monomer−dimer equilibrium at 4 °C and pH 7.5 (*20*). With these two studies in mind, we hypothesized that ClpA may reside in a monomer−dimer−tetramer equilibrium at all temperatures, but the self-association equilibrium constants depend on temperature in such a way that only monomers and tetramers are observed at 25 °C but other oligomeric states may be more significantly populated at different temperatures. Such an observation would not be without precedence, as other self-associating protein systems have exhibited changes in the population distribution as a function of temperature (*21*). Furthermore, temperature is well-known to alter assembly states of other biological macromolecules (*22*−*25*).

Here we report a detailed examination of the ClpA self-association reaction as a function of temperature. To accomplish this, we have examined the self-assembly reaction at 11 temperatures between 3.9 and 38.2 °C using sedimentation velocity and sedimentation equilibrium techniques. The result of this examination reveals that the ClpA self-association reaction can be modeled by a monomer−dimer−tetramer equilibrium over the temperature range examined. However, the dimeric species is only significantly populated at ∼4 and ∼38 °C.

MATERIALS AND METHODS

Buffers. Buffers were prepared with reagent grade chemicals using doubly distilled H_2O. Doubly distilled water was produced using the Purelab Ultra Genetic system (Siemens Water Technology). Buffer H consists of 25 mM HEPES, 300 mM NaCl, 10 mM $MgCl_2$, 2 mM 2-mercaptoethanol, and 10% (v/v) glycerol (pH 7.5) at the temperature indicated in the text. ClpA was purified as previously described (*19*). The ClpA concentration was determined spectrophotometrically using an extinction coefficient of $(3.1 \pm 0.2) \times 10^4\ M^{-1}\ cm^{-1}$ for the monomer as described previously (*19*).

Analytical Ultracentrifugation. Analytical ultracentrifugation experiments, both sedimentation velocity and sedimentation equilibrium, were performed using a Beckman XL-A analytical ultracentrifuge. Sedimentation velocity experiments were performed by loading a sample of protein (380 μL) into a double-sector Epon charcoal-filled centerpiece and subjected to an angular velocity of 40000 rpm. Absorbance scans as a function of radial position were collected by scanning the sample cells at a wavelength of 280 nm at intervals of 0.002 cm. Scans were collected every 4 min.

Sedimentation equilibrium experiments were performed by loading a sample of protein (110 μL) into a double-sector Epon charcoal-filled centerpiece. Samples were sedimented at the velocity indicated in the text until sedimentation equilibrium was achieved as judged by WinMatch (*26*). Speeds of 12000, 15000, and 18000 rpm were used to obtain sedimentation equilibrium data. Absorbance versus radial position scans were taken at 280 nm. ClpA concentrations were chosen so that a wide range of ClpA association states could be surveyed. No fewer than five concentrations and three speeds were used per each temperature examined, yielding a minimum of 15 data sets. Sedimentation equilibrium data were analyzed using HeteroAnalysis (*27*).

Temperature Calibration of the Beckman XL-A Analytical Ultracentrifuge. The chamber temperature of the Beckman XL-A analytical ultracentrifuge was calibrated using a mixture of $CoCl_2 \cdot 6H_2O$ and ethanol as previously described (*28*). The data were described by the linear equation $y = -2.33 + 1.11x$, were y is the XL-A temperature control setting and x is the temperature within the chamber. All temperatures reported in this paper are reported as the temperature in the chamber.

Analysis of Sedimentation Velocity Data. Sedimentation velocity boundaries were analyzed using SedFit, where SedFit generates a $c(s)$ distribution of Lamm equation solutions (*29*). Sedimentation velocity boundaries were also analyzed using DCDT+ version 2.2.1 to generate normalized $g(s^*)$ distributions (*30*, *31*). The sedimentation coefficient, s, is given by Svedberg's equation (eq 1)

$$s = \frac{M(1-\bar{v}\rho)}{Nf} = \frac{MD(1-\bar{v}\rho)}{RT} \quad (1)$$

where M is the molecular mass, $\bar{v}$ is the partial specific volume of the macromolecule, ρ is the density of the buffer, N is Avogadro's number, f is the frictional coefficient, D is the diffusion coefficient, R is the ideal gas constant, and T is the absolute temperature. The two forms of eq 1 are related by eq 2

$$D = \frac{k_b T}{f} \quad (2)$$

where k_b is Boltzman's constant. For comparison to previously reported weight average sedimentation coefficients, the weight average sedimentation coefficient was calculated from the $g(s^*)$ distribution by integration over the area of the $g(s^*)$ species distribution (*32*, *33*). All sedimentation coefficients reported in the text are corrected to 20 °C and infinite dilution in water, $s_{20,w}$, using standard equations in DCDT+ (*30*, *31*, *34*).

Analysis of Sedimentation Equilibrium Data. Sedimentation equilibrium boundaries were subjected to global NLLS[1] fitting using HeteroAnalysis (*27*). Using HeteroAnalysis, absorbance scans as a function of radial position were fit to a sum of exponentials, where each exponential represents a discrete population of an oligomeric species (n-mer) formed from n monomeric units (eq 3)

$$A_T = \sum_{i=1}^{j} A_{f,ref}^{n_i} L_{n_i 0,\,Abs} e^{n_i \sigma \xi} + b \quad (3)$$

where A_T is the total absorbance at radial position r, j is the number of species, n_1 always equals 1, n_i is the number of monomers in an oligomer, $A_{f,ref}$ is the absorbance of the monomeric species at the reference radial position, r_0, $\xi = (r^2 - r_0^2)/2$, b is a baseline offset term, and σ is the reduced molecular mass of the monomeric species given by eq 4

$$\sigma = \frac{M(1-\bar{v}\rho)\omega^2}{RT} \quad (4)$$

where M is the molecular mass of the monomer, $\bar{v}$ is the partial specific volume of the monomer, ρ is the density of the solvent, ω is the angular velocity of the rotor, R is the ideal gas constant, and T is the absolute temperature.

[1]Abbreviations: NLLS, nonlinear least-squares.

Table 1: Values of Partial Specific Volume ($\bar{v}$) and Density Used in This Temperature Survey

temp (°C)	$\bar{v}$	$\bar{v}$ (corrected for 10% glycerol)	ρ (g/mL)
3.9	0.7313	0.7346	1.04379
5.7	0.7321	0.7354	1.04377
8.4	0.7332	0.7365	1.04364
11.1	0.7344	0.7377	1.04334
15.6	0.7363	0.7396	1.04278
20.1	0.7382	0.7415	1.04192
21.9	0.7390	0.7423	1.04152
24.7	0.7401	0.7434	1.04082
29.2	0.7421	0.7454	1.03953
35.5	0.7447	0.7480	1.03741
38.2	0.7459	0.7492	1.03640

The partial specific volume, $\bar{v}$, of ClpA was calculated from the primary sequence at the correct chamber temperature using SEDNTERP version 1.09, revision level 1.2 (D. Hayes, Magdalen College; T. Laue, University of New Hampshire; J. Philo, Alliance Protein Laboratories) (*35*). The value of $\bar{v}$ was also corrected for the inclusion of 10% glycerol according to eq 5 (*36*).

$$\frac{\Delta\bar{v}}{\Delta[\text{glycerol}]\%\ (\text{v/v})} = (3.33 \pm 0.38) \times 10^{-4}\ \text{mL/g} \qquad (5)$$

For the 10% glycerol used in our experiments, this results in a correction $\Delta\bar{v}$ of 0.0033 mL/g, which results in a 0.45% increase in $\bar{v}$ (see Table 1). This was verified at 3.9, 24.7, and 38.2 °C by performing global NLLS analysis, using HeteroAnalysis to fit sedimentation equilibrium data by allowing the buoyant molecular mass $M^* = M(1 - \bar{v}\rho)$ for the monomer to float as a fitting parameter and using the calculated density, ρ, and molecular mass of the monomer to solve for the partial specific volume, $\bar{v}$. Following this procedure, the partial specific volume was found to be 0.7369, 0.7370, and 0.7438 at 3.9, 24.7, and 38.2 °C, respectively, which is less than 1% different from the value calculated in SEDNTERP with or without the correction for glycerol given in eq 5 (see Table 1). The percent deviation in partial specific volume measured here is consistent with what others have observed (*37*, *38*). Thus, the values for partial specific volume calculated using SEDNTERP at the appropriate temperature and presented in Table 1 were used in the NLLS analysis.

The density of the buffer, ρ, was also calculated for H300 using SEDNTERP (see Table 1). Because SEDNTERP does not include 2-mercaptoethanol, the density was calculated by excluding 2-mercaptoethanol. In an attempt to determine the impact of excluding 2-mercaptoethanol in our calculation of density, we reasoned that because DTT is essentially two 2-mercaptoethanol molecules fused together it could serve as a model compound. It was found that inclusion of 2 mM DTT in the calculation affected the density in the fifth decimal place, which results in an ~0.001% deviation in density. Thus, we conclude that exclusion of 2-mercaptoethanol in our calculation of density is insignificant.

Finally, in our buffer system, the dominant component that affects density is inclusion of 10% glycerol. To determine the uncertainty in the glycerol concentrations, we checked the glycerol concentration by comparing the refractive index of 10% (v/v) glycerol with reported values (*39*). We determined that the uncertainty in the glycerol concentration is 10.00 ± 0.01% (v/v). This uncertainty results in a 0.003% uncertainty in the density.

To determine how the uncertainty in partial specific volume and density may propagate into a calculation of molecular mass, we solved eq 4 for molecular mass as given by eq 6.

$$M = \frac{\sigma RT}{(1 - \bar{v}\rho)\omega^2} \qquad (6)$$

The uncertainty in both $\bar{v}$ and ρ will propagate into a calculation of molecular mass according to eq 7

$$\delta M = \sqrt{\left(\frac{\partial M}{\partial \bar{v}}\,\delta\bar{v}\right)^2 + \left(\frac{\partial M}{\partial \rho}\,\delta\rho\right)^2} \qquad (7)$$

where δM is the uncertainty in the molecular mass, $\delta\bar{v}$ is the uncertainty in the partial specific volume, and $\delta\rho$ is the uncertainty in density (*40*). Upon execution of the derivatives in eq 7, one acquires eq 8.

$$\delta M = \sqrt{\left[\frac{\sigma RT\rho}{(1 - \bar{v}\rho)^2\omega^2}\,\delta\bar{v}\right]^2 + \left[\frac{\sigma RT\bar{v}}{(1 - \bar{v}\rho)\omega^2}\,\delta\rho\right]^2} \qquad (8)$$

Table 1 shows that the partial specific volume varies from 3.9 to 38.2 C by 1.9% and the density varies over the same range of temperature by 0.7%. Thus, 1.9 and 0.7% represent the largest potential uncertainties in partial specific volume and density used in this study, respectively. Using these estimates for uncertainty in both partial specific volume and density reveals a 7.6% uncertainty in the molecular mass determination, which would be 84200 ± 6400 Da for a monomer of ClpA.

In eq 3, $L_{n,0,\text{Abs}}$ is the equilibrium constant in absorbance units for n monomers associating to form an n-mer (eq 9).

$$L_{n,0,\text{Abs}} = \frac{A_n}{A_{\text{mon}}{}^n} \qquad (9)$$

where A_n is the absorbance of an n-mer and A_{mon} is the absorbance of the free monomer. The equilibrium constant in concentration units, $L_{n,0}$, is determined by substituting Beer's law into eq 9 and rearranging to yield eq 10.

$$L_{n,0} = L_{n,0,\text{Abs}}\frac{\varepsilon^{n-1}l^{n-1}}{n} \qquad (10)$$

Further Analysis of Equilibrium Constants Determined by Sedimentation Equilibrium Experiments. $L_{4,0}$ values determined from NLLS analysis with $L_{2,0}$ constrained were plotted as a function of inverse temperature. This interpretation of the data resulted in a nonlinear van't Hoff plot. The nonlinear van't Hoff plot was subjected to NLLS analysis using eq 11

$$\ln K = \frac{\Delta C_p^\circ}{R}\left[\ln\left(\frac{T}{T_S}\right) + \frac{T_H}{T} - 1\right] \qquad (11)$$

where T_S is the temperature at which $\Delta S^\circ = 0$, T_H is the temperature at which $\Delta H^\circ = 0$, and ΔC_p° is the observed change in heat capacity at a constant pressure.

Weight average sedimentation coefficients, $s_{20,w}$, as a function of free ClpA concentration were analyzed using eq 12 (*41*)

$$\bar{s}_{20,w} = (s_{m,20,w} + 2s_{d,20,w}L_{2,0}[\text{ClpA}]_{\text{free}} + 4s_{t,20,w}L_{4,0}[\text{ClpA}]_{\text{free}}{}^3)/(1 + 2L_{2,0}[\text{ClpA}]_{\text{free}} + 4L_{4,0}[\text{ClpA}]_{\text{free}}{}^3) \qquad (12)$$

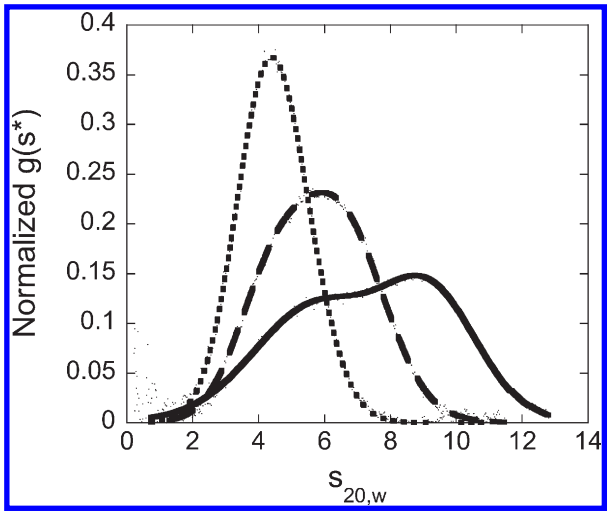

FIGURE 1: Normalized $g(s^*)$ profiles as a function of ClpA concentration at 24.7 °C. Normalized $g(s^*)$ profiles for 1 (···), 9 (– – –), and 18 μM ClpA (—) in buffer H at pH 7.5 and 24.7 °C.

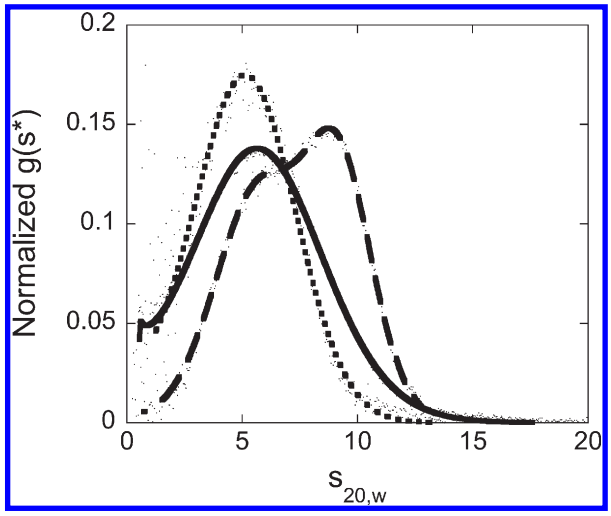

FIGURE 2: Normalized $g(s^*)$ profiles for 18 μM ClpA as a function of temperature. Normalized $g(s^*)$ profiles for 18 μM ClpA in buffer H (pH 7.5 at the appropriate temperature) at 3.9 (···), 24.7 (– – –), and 38.2 °C (—).

where eq 12 relates the weight average $s_{20,w}$ to the free ClpA concentration, $s_{m,w,20}$ represents the monomer sedimentation coefficient, $s_{d,w,20}$ represents the dimer sedimentation coefficient, $s_{t,w,20}$ represents the tetramer sedimentation coefficient, and $L_{2,0}$ and $L_{4,0}$ are defined by eqs 13–16.

$$2\text{ClpA} \overset{L_{2,0}}{\rightleftharpoons} \text{ClpA}_2 \quad (13)$$

$$4\text{ClpA} \overset{L_{4,0}}{\rightleftharpoons} \text{ClpA}_4 \quad (14)$$

$$L_{2,0} = \frac{[\text{ClpA}_2]}{[\text{ClpA}]_{\text{free}}^{\,2}} \quad (15)$$

$$L_{4,0} = \frac{[\text{ClpA}_4]}{[\text{ClpA}]_{\text{free}}^{\,4}} \quad (16)$$

To relate the free ClpA concentration to the total ClpA concentration, we used the conservation of mass equation (eq 17), where $[\text{ClpA}]_t$ is the total ClpA concentration.

$$[\text{ClpA}]_t = [\text{ClpA}]_{\text{free}} + 2L_{2,0}[\text{ClpA}]_{\text{free}}^{\,2} + 4L_{4,0}[\text{ClpA}]_{\text{free}}^{\,4} \quad (17)$$

The weight average sedimentation coefficient as a function of the total ClpA concentration and cell temperature, shown in Figure 3A–C, was subjected to NLLS analysis by implicitly solving eqs 12 and 17. This was accomplished using the implicit fitting routine in Micromath Scientist (Micromath, St. Louis, MO).

RESULTS

Sedimentation Velocity Experiments to Examine the Effect of Temperature on the Hydrodynamic Properties of ClpA. Sedimentation velocity experiments were performed with 1, 9, and 18 μM ClpA in buffer H (pH 7.5 at 24.7 °C) as described in Materials and Methods. Figure 1 shows the results of $g(s^*)$ analysis of the sedimentation velocity boundaries. The $g(s^*)$ distribution clearly exhibits a broadening reaction boundary as the concentration of ClpA increases. The analysis resulted in weight average $s_{20,w}$ values of 4.42 ± 0.07, 5.92 ± 0.08, and 7.26 ± 0.06 S at 1, 9, and 18 μM ClpA, respectively. This result shows a concentration-dependent assembly of ClpA, with multiple species clearly present at 18 μM ClpA. We have previously shown that this reaction boundary can be described by a mixture of monomers and tetramers of ClpA at 25 °C (*19*).

To begin examining the effect of temperature on the self-association reaction, we performed sedimentation velocity experiments at 3.9, 24.7, and 38.2 °C. Figure 2 shows the result of $g(s^*)$ analysis of sedimentation velocity experiments performed with 18 μM ClpA at each temperature in buffer H (pH 7.5 at the indicated temperature). At 18 μM ClpA, one can see a clear difference in the reaction boundary upon comparison of the 24.7 °C experiment to the 3.9 and 38.2 °C experiments. In addition to the visual change in the reaction boundaries, the weight average $s_{20,w}$ values show a significant change at the extremes of temperature. That is to say, at 24.7 °C a weight average $s_{20,w}$ of 7.26 ± 0.06 S is observed, whereas the weight average $s_{20,w}$ decreases to 4.96 ± 0.20 and 5.87 ± 0.06 S at 3.9 and 38.2 °C, respectively.

We propose two potential possibilities that could describe the observed change in weight average $s_{20,w}$ with temperature. Either there is a change in the assembly state from monomer–tetramer at ~25 °C to monomer–dimer or monomer–trimer at other temperatures, or at the single concentration of 18 μM ClpA, the monomer–tetramer equilibrium constant is weaker and thus there is an apparent shift to lower weight average sedimentation coefficient values. Protein denaturation does not likely describe the observed change in sedimentation coefficient as a function of temperature because differential scanning calorimetry (DSC) experiments do not exhibit any change in the protein until >45 °C (data not shown). Moreover, enzymatic activity is observed over the full range of temperatures examined here (B. Rajendar, manuscript in preparation) (*17*).

To further examine the apparent changes in the weight average sedimentation coefficient as a function of temperature, sedimentation velocity experiments were performed at 11 temperatures (3.9, 5.7, 8.4, 11.1, 15.6, 20.1, 21.9, 24.7, 29.2, 35.5, and 38.2 °C) at 1, 9, and 18 μM ClpA. Each experiment was subjected to $g(s^*)$ analysis, and Figure 3 displays the weight average sedimentation coefficient, $s_{20,w}$, for each of these concentrations as a function of temperature. At 1 μM ClpA (Figure 3A), the weight average $s_{20,w}$ values are approximately the same across the 3.9–38.2 °C temperature range, falling between 3.5 and 4.5 S. This result most likely represents monomeric ClpA at all temperatures

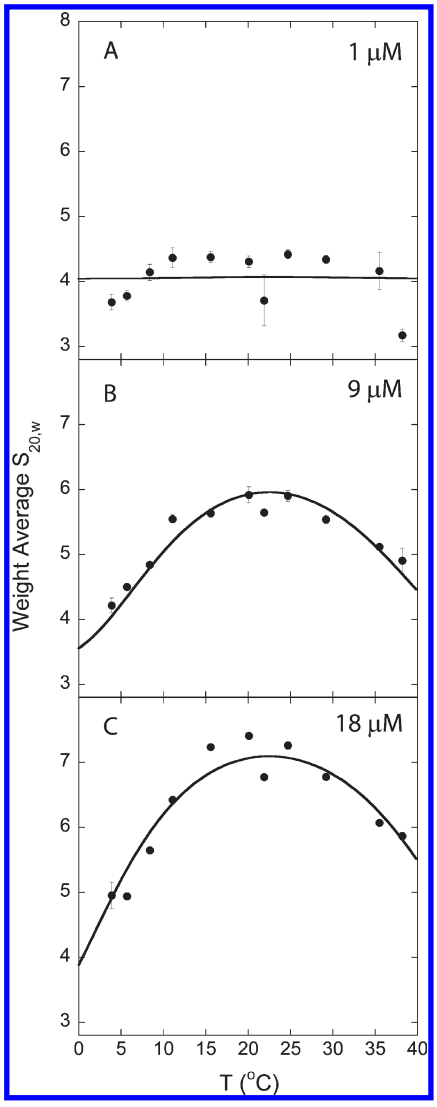

FIGURE 3: Plots of weight average $s_{20,w}$ vs temperature for (A) 1, (B) 9, and (C) 18 μM ClpA in buffer H at temperatures from 3.9 to 38.2 °C. The solid lines represent the results of the global nonlinear least-squares fits of the data for all three concentrations via combination of eqs 11, 12, and 17. From this analysis, $T_S = 30.4 \pm 1.4$ °C, $T_H = 22.5 \pm 0.7$ °C, $\Delta C_p^\circ{}_{obs} = -2.61 \pm 0.61$ kcal K^{-1} (mol of tetramer)$^{-1}$, $s_{m,20,w} = 4.13 \pm 0.16$ S, and $s_{t,20,w} = 9.94 \pm 1.25$ S.

because we have previously shown that only monomeric ClpA is present at 1 μM and 25 °C (*19*). In contrast, when the ClpA concentration is increased to 9 μM (Figure 3B), lower values of $s_{20,w}$ between 4.2 and 5.1 S are observed at the extremes of the temperature range (3.9−8.4 and 35.5−38.2 °C) compared to an $s_{20,w}$ of 5.5−6.0 S measured between 11.1 and 29.2 °C. Finally, at 18 μM ClpA (Figure 3C), a distinct curvature is observed in the plot of weight average sedimentation coefficient versus temperature, resembling a parabola. Similar to the 9 μM data in Figure 3B, the 18 μM data in Figure 3C show lower weight average sedimentation coefficient values between 5.0 and 6.0 S in the high and low temperature range and higher sedimentation coefficient values between 6.4 and 7.4 S from 11.1 to 29.2 °C.

The simplest explanation for the nonlinear dependence of the weight average sedimentation coefficient is a temperature-dependent enthalpy change for the monomer−tetramer self-assembly reaction, i.e., a significant heat capacity change, ΔC_p°. Alternatively, we have previously shown that ClpA resides in a monomer−tetramer equilibrium at 25 °C. However, this previous conclusion does not rule out the possibility that a smaller oligomeric intermediate exists, but only that a smaller intermediate, if present, is not significantly populated at thermodynamic equilibrium at 25 °C. Thus, as the temperature is decreased or increased, an oligomer smaller than a tetramer, e.g., dimer, may become significantly populated. That is to say, the combination of the temperature dependence of the monomer to *n*-mer equilibrium constant and the monomer to tetramer equilibrium constant may depend on temperature in such a way that it yields the observed nonlinear dependence on temperature.

Examination of the Effect of Temperature on the Assembly State of ClpA by Sedimentation Equilibrium. To resolve these possibilities, sedimentation equilibrium experiments were performed to determine the assembly state and equilibrium constants as a function of temperature. Experiments were conducted as described in Materials and Methods with 4, 6, 9, 15, 18, and 22 μM ClpA at 3.9, 5.7, 8.4, 11.1, 15.6, 20.1, 21.9, 24.7, 29.2, 35.5, and 38.2 °C (*27*). Figure 4 displays a representative set of sedimentation equilibrium data collected at 3.9 °C.

Each set of sedimentation equilibrium data collected at a given temperature was subjected to NLLS analysis with a model containing two species as given by eq 3 where $j = 2$. In this analysis, the monomer molecular mass was constrained to 84200 Da, i.e., the molecular mass calculated from sequence and determined previously (*19*). Each set of data is described well by a monomer−*n*-mer model as judged by a distribution of residuals similar to that shown in Figure 4 and the comparable root-mean-square deviation (rmsd) reported in Table 2 for each temperature. Systematic residuals were observed in attempts to describe the data by a single ideal species (eq 3) where $j = 1$.

Figure 5 is a plot of the number of monomers in an oligomer, n_2, determined from the analysis at each temperature. At temperatures of 15.6, 20.1, 21.9, 24.7, and 29.2 °C, $n_2 \sim 4$, which is consistent with a tetramer of ClpA as previously observed at 25 °C (*19*). Consistently, $g(s^*)$ analysis of sedimentation velocity experiments performed at these five temperatures also revealed a higher weight average $s_{20,w}$ value (see Figure 3C). Strikingly, the six remaining temperatures examined (3.9, 5.7, 8.4, 11.1, 35.5, and 38.2 °C) result in an n_2 of ~3, consistent with a trimer of ClpA. This result is also consistent with sedimentation velocity experiments, where the $g(s^*)$ analysis revealed a lower weight average sedimentation coefficient (see Figure 3C). Table 2 reports the results of the analysis of all of the sedimentation equilibrium data when each set of data collected at a given temperature is subjected to NLSS analysis using a monomer−*n*-mer model (eq 3) where $j = 2$, with n_2 constrained to the nearest integer value, i.e., $n_2 = 3$ or 4.

The NLLS analysis of the sedimentation equilibrium reveals that at low and high temperatures the data can be described by a monomer−trimer equilibrium, whereas the intermediate-temperature data can be described by a monomer−tetramer equilibrium (see Table 2). The existence of a trimer−tetramer transition as a function of temperature seems unlikely. A more likely explanation is the presence of a dimeric species, with values of the monomer−dimer equilibrium constant, $L_{2,0}$, being such that the presence of a dimer is obscured at some temperatures. For example, we previously showed that at 25 °C sedimentation equilibrium data were best described by a monomer−tetramer model, which is consistent with the data presented here (*19*). However, it is possible that a dimeric intermediate exists, but the monomer−dimer equilibrium constant is much weaker than the monomer−tetramer equilibrium constant; thus, we do not,

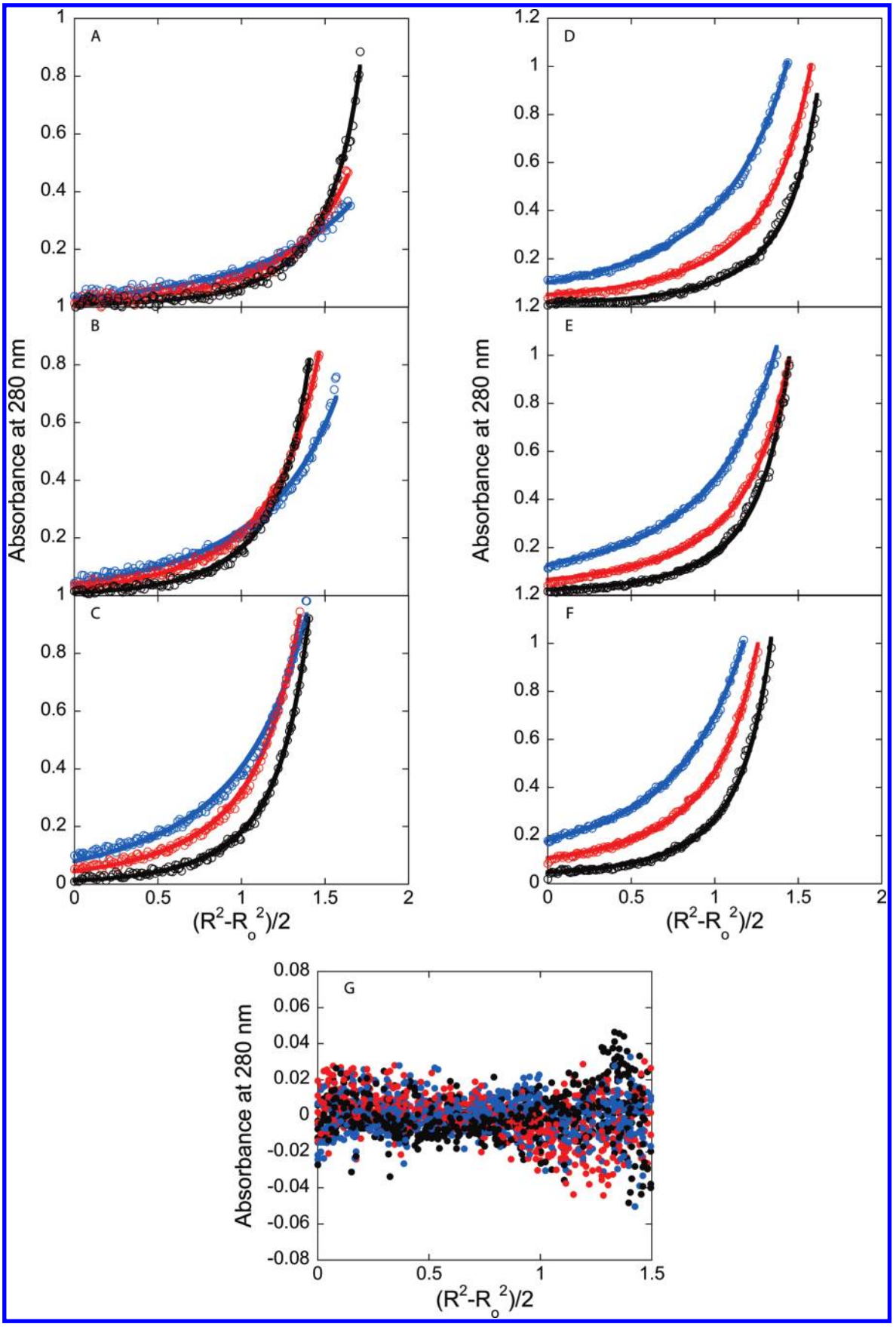

FIGURE 4: Sedimentation equilibrium raw data (3.9 °C) along with global fits for (A) 4, (B) 6, (C) 9, (D) 15, (E) 18, and (F) 22 μM ClpA collected at 3.9 °C at 12000 (blue), 15000 (red), and 18000 rpm (black). Experimental data were analyzed as described in Materials and Methods. Absorbance scans were collected at 280 nm. Empty circles represent experimental data points, while solid lines represent the results of the global NLLS fit using eq 3 with the following parameters: $n_2 = 2$, $n_3 = 4$, $L_{2,0} = (1.32 \pm 0.01) \times 10^4$ M^{-1}, and $L_{4,0} = (2.19 \pm 0.02) \times 10^{13}$ M^{-3}. (G) Residuals for the global NLLS fit.

Table 2: $L_{n,0}$ and rmsd Values as a Function of Temperature[a]

temp (°C)	n_2	$L_{n2,0}$ [$M^{-(n_2-1)}$]	rmsd
3.9	3	$(7.21 \pm 0.3) \times 10^8$	0.01224 ± 0.0010
5.7	3	$(9.77 \pm 6.4) \times 10^8$	0.01414 ± 0.0065
8.4	3	$(2.06 \pm 1.3) \times 10^9$	0.01346 ± 0.0023
11.1	3	$(2.41 \pm 1.5) \times 10^9$	0.01339 ± 0.0058
15.6	4	$(1.47 \pm 0.4) \times 10^{14}$	0.01324 ± 0.0014
20.1	4	$(9.28 \pm 3.3) \times 10^{13}$	0.01001 ± 0.0004
21.9	4	$(8.79 \pm 1.4) \times 10^{13}$	0.01267 ± 0.0048
24.7	4	$(2.16 \pm 0.1) \times 10^{14}$	0.00944 ± 0.0003
29.2	4	$(5.55 \pm 2.5) \times 10^{13}$	0.01430 ± 0.0007
35.5	3	$(1.20 \pm 0.1) \times 10^9$	0.01611 ± 0.0012
38.2	3	$(9.18 \pm 0.1) \times 10^8$	0.00953 ± 0.0018

[a]Values are the average of three independent sedimentation equilibrium runs per temperature. Uncertainties represent the standard deviation from three independent analysis.

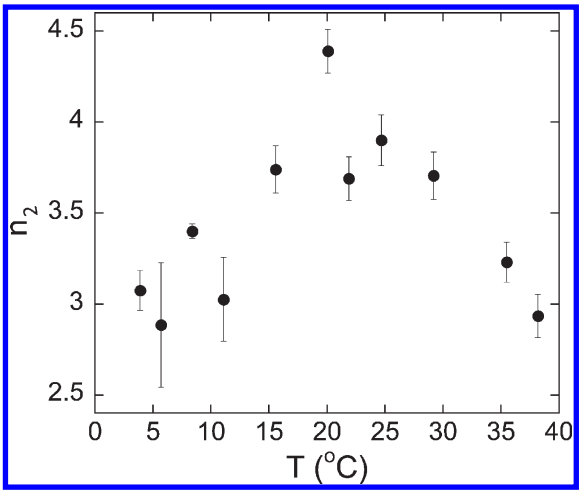

FIGURE 5: Molecular mass of ClpA oligomer as a function of experimental temperature. Multiple sedimentation equilibrium experiments were performed at 3.9, 5.7, 8.4, 11.1, 15.6, 20.1, 21.9, 24.7, 29.2, 35.5, and 38.2 °C with 4, 6, 9, 15, 18, and 22 μM ClpA at 12000, 15000, and 18000 rpm. The resulting data were fit to a monomer−*n*-mer model (eq 3) where $j = 2$, with the monomer value constrained to 84200 Da and the value of n_2 varied. The experimentally determined values for n_2 are plotted as a function of temperature.

experimentally, observe a significant population of dimers at thermodynamic equilibrium. However, if the value of the dimeric equilibrium constant approaches the value of the tetrameric equilibrium constant and the data are examined by a two-state model (i.e., monomer−*n*-mer), then one will observe an apparent shift to a lower molecular mass because of the averaging of the two oligomers. We have previously illustrated this possibility with simulations (*19*). Further, the two equilibrium constants will certainly depend upon temperature, and the most likely explanation for an apparent shift to trimers at both high and low temperatures is that the two equilibrium constants depend upon temperature in such a way that dimers are more significantly populated at the two extremes of temperature; i.e., the value of $L_{2,0}$ approaches the value of $L_{4,0}$. Thus, one observes an apparent trimer, which is really an averaging of the population of dimers and tetramers.

Fit of Sedimentation Equilibrium Data as a Function of Temperature to a Monomer−Dimer−Tetramer Model. To examine the possibility of a dimeric intermediate being present at all temperatures and the apparent shift to a tetramer being due to averaging of the populations of dimers and tetramers, we used an alternative method of fitting the sedimentation equilibrium data as a function of temperature. Sedimentation equilibrium data collected at each temperature were subjected to NLLS analysis to a monomer−dimer−tetramer model, described by eq 3, where $j = 3$, $n_2 = 2$, and $n_3 = 4$ and the equilibrium constants $L_{2,0}$ and $L_{4,0}$ are defined in eqs 13−16. Markedly, the 3.9 and 38.2 °C data sets were successfully described by a monomer−dimer−tetramer model by allowing all parameters to float. The solid lines in Figure 4 represent the result of a global NLLS analysis of the sedimentation equilibrium data collected at 3.9 °C to a monomer−dimer−tetramer model that yielded equilibrium constants $L_{2,0} = (1.32 \pm 0.01) \times 10^4\ M^{-1}$, $L_{4,0} = (2.19 \pm 0.02) \times 10^{13}\ M^{-3}$, and an rmsd of 0.01164. Likewise, when the data collected at 38.2 °C were subjected to NLLS analysis using a monomer−dimer−tetramer model, the following values were found: $L_{2,0} = (1.97 \pm 0.03) \times 10^4\ M^{-1}$, $L_{4,0} = (1.20 \pm 0.01) \times 10^{14}\ M^{-3}$, and rmsd = 0.01004. Interestingly, at all other temperatures, $L_{2,0}$ was not well constrained and the NLLS analysis always resulted in a two-species fit; i.e., the data are best described by a monomer−*n*-mer model.

Table 3: $L_{4,0}$ as a Function of Temperature When $L_{2,0}$ Is Constrained to $1.5 \times 10^4\ M^{-3}$[a]

temp (°C)	$L_{2,0}$ (M^{-1})	$L_{4,0}$ (M^{-3})	rmsd
3.9	1.5×10^4	$(2.33 \pm 0.2) \times 10^{13}$	0.01233 ± 0.0009
5.7	1.5×10^4	$(3.93 \pm 3.7) \times 10^{13}$	0.01415 ± 0.0067
8.4	1.5×10^4	$(7.84 \pm 0.1) \times 10^{13}$	0.01134 ± 0.0007
11.1	1.5×10^4	$(7.06 \pm 3.0) \times 10^{13}$	0.01378 ± 0.0052
15.6	1.5×10^4	$(2.09 \pm 0.4) \times 10^{14}$	0.00998 ± 0.0006
20.1	1.5×10^4	$(1.26 \pm 0.4) \times 10^{14}$	0.00998 ± 0.0006
21.9	1.5×10^4	$(1.20 \pm 0.1) \times 10^{14}$	0.01279 ± 0.0044
24.7	1.5×10^4	$(3.00 \pm 0.1) \times 10^{14}$	0.00945 ± 0.0002
29.2	1.5×10^4	$(9.89 \pm 4.5) \times 10^{13}$	0.01448 ± 0.0005
35.5	1.5×10^4	$(4.36 \pm 0.6) \times 10^{13}$	0.01609 ± 0.0011
38.2	1.5×10^4	$(3.68 \pm 0.9) \times 10^{13}$	0.00959 ± 0.0018

[a]Values are the average of three independent sedimentation equilibrium runs per temperature. Uncertainties represent the standard deviation from three independent analysis.

These observations suggest that either the dimerization equilibrium constant, $L_{2,0}$, is constant as a function of temperature or $L_{2,0}$ exhibits a temperature dependence that always results in $L_{4,0} \gg L_{2,0}$ at all the observed temperatures other than 3.9 and 38.2 °C, subsequently causing the dimeric species not to be populated sufficiently to be well constrained in the NLLS analysis. With this observation in mind, we subjected the remaining data collected between 3.9 and 38.2 °C to NLLS analysis using a monomer−dimer−tetramer model with an $L_{2,0}$ of $1.5 \times 10^4\ M^{-1}$ and $L_{4,0}$ varied as a fitting parameter. This $L_{2,0}$ value of $1.5 \times 10^4\ M^{-1}$ was chosen for two reasons. First, from simulations we previously showed that this value represents the upper limit for $L_{2,0}$ at 25 °C (*19*). Second, it is approximately the measured value of $L_{2,0}$ at both 3.9 and 38.2 °C. Table 3 reports the obtained values of $L_{4,0}$ and associated rmsd values. The experimental data are equally well described by a monomer−dimer−tetramer model and a monomer−*n*-mer model as judged by comparison of the rmsd values for the monomer−*n*-mer fit to the monomer−dimer−tetramer fit (i.e., Table 2 compared to Table 3, respectively).

Figure 6 displays the resulting tetramerization equilibrium constant, $L_{4,0}$, values plotted as a function of inverse temperature ($1/T$) and shows that the equilibrium constant clearly exhibits a nonlinear dependence on inverse temperature. Such a result

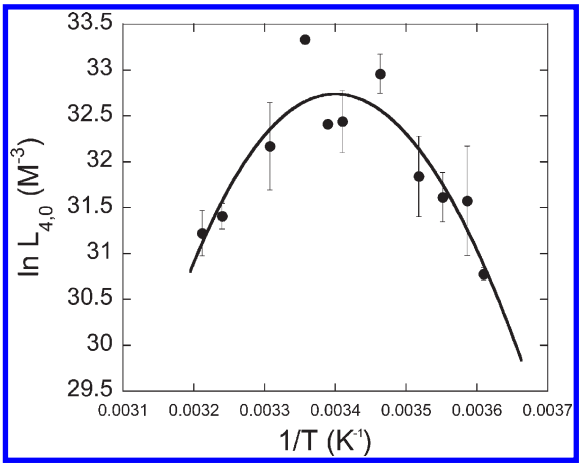

FIGURE 6: van't Hoff plot of the tetramerization equilibrium constant. Multiple sedimentation equilibrium experiments were performed at 3.9, 5.7, 8.4, 11.1, 15.6, 20.1, 21.9, 24.7, 29.2, 35.5, and 38.2 °C with 4, 6, 9, 15, 18, and 22 μM ClpA at 12000, 15000, and 18000 rpm. The resulting data were fit to a monomer−dimer−tetramer model (eqs 13−16), with $L_{2,0}$ constrained to 1.5×10^4 M^{-1}. A van't Hoff plot was made of the resulting $L_{4,0}$ values (●).The data were fit to eq 11 (resulting in the solid line), and the following values were obtained: $T_S = 30.5 \pm 2.0$ °C, $T_H = 21.0 \pm 0.9$ °C, and $\Delta C_p^\circ = -2.03 \pm 0.35$ kcal K^{-1} (mol of tetramer)$^{-1}$.

suggests a significant heat capacity change (*42*). Such a nonlinear van't Hoff plot can be described by eq 11, assuming a temperature-independent heat capacity change (*21*, *43*). The equilibrium constant, $L_{4,0}$, versus inverse temperature, shown in Figure 6, was subjected to NLLS analysis using eq 7. The following resultant values were obtained: $T_S = 30.5 \pm 2.0$ °C, $T_H = 21.0 \pm 0.9$ °C, and $\Delta C_p^\circ{}_{obs} = -2.03 \pm 0.35$ kcal K^{-1} (mol of tetramer)$^{-1}$.

Modeling of the Weight Average Sedimentation Coefficient as a Function of Temperature. Sedimentation equilibrium experiments reveal that the ClpA self-association reaction can be modeled with a monomer−dimer−tetramer model over the temperature range of ~4−38 °C. Thus, the weight average sedimentation coefficient collected at 1, 9, and 18 μM ClpA over a range of temperatures shown in Figure 3 should be able to be described via combination of eqs 11, 12, and 17. First, eq 11 describes the temperature dependence of the tetramerization equilibrium constant, $L_{4,0}$. Second, eq 12 describes the ClpA concentration dependence of the weight average sedimentation coefficient. Finally, eq 17 relates the free ClpA monomer concentration to the total ClpA concentration.

The weight average sedimentation coefficient as a function of ClpA concentration and temperature, shown in Figure 3, was subjected to global NLLS analysis using eqs 11, 12, and 17 by constraining $L_{2,0}$ to 1.5×10^4 M^{-1}. Once these three equations are combined, both ClpA concentration and temperature are independent variables, and T_S, T_H, $\Delta C_p^\circ{}_{obs}$, $s_{m,20,w}$, $s_{d,20,w}$, and $s_{t,20,w}$ are parameters (see Materials and Methods). The solid lines in Figure 3A−C are the result of the NLLS analysis via combination of eqs 11, 12, and 17. From this analysis, $T_S = 30.4 \pm 1.4$ °C, $T_H = 22.5 \pm 0.7$ °C, and $\Delta C_p^\circ{}_{obs} = -2.61 \pm 0.61$ kcal K^{-1} (mol of tetramer)$^{-1}$. These values correspond well with those obtained from the analysis of $L_{4,0}$ as a function of inverse temperature shown in Figure 6. Additionally, it is interesting that from this fit $s_{20,w}$ values of 4.13 ± 0.16 S for ClpA monomers and 9.94 ± 1.25 S for ClpA tetramers are obtained, values quite similar to previously reported results (*19*). The terms describing the dimer were not well determined in the fit and thus were considered negligible.

DISCUSSION

The molecular chaperone, ClpA, is a complex allosteric machine. As we have shown here, the protein resides in a mixture of monomers, dimers, and tetramers in the absence of a nucleotide. Previous work has shown that upon nucleoside triphosphate binding, ClpA assembles into hexameric ring structures with ATP-driven protein unfolding activity (*14*, *20*). However, to rigorously examine the energetics of nucleotide binding and nucleotide-induced hexamer formation, one must have a model that accurately describes the self-association equilibrium in the absence of nucleotide. Here we have shown that the self-association reaction can be modeled by a monomer−dimer−tetramer equilibrium from ~4 to 38 °C. With this model in hand, a rigorous examination of the ligand-linked assembly reaction is underway.

The Assembly State of ClpA Is Best Described as a Monomer−Dimer−Tetramer Equilibrium. We recently reported that ClpA resides in a monomer−tetramer equilibrium at 25 °C in the absence of a nucleotide (*19*). As discussed, this conclusion does not rule out the possibility that dimers exist; it says only that dimers are not significantly populated at 25 °C. Nevertheless, this observation appears to be in stark contrast to the previously published results, of others, that concluded ClpA is in a monomer−dimer equilibrium in the absence of a nucleotide. However, the previous studies were performed at 4 °C compared to our experiments that were performed at 25 °C (*19*, *20*). In an attempt to reconcile our observations at 25 °C with the previous observations at 4 °C, we initiated an examination of the temperature dependence of self-association. Sedimentation velocity experiments revealed that the weight average sedimentation coefficient decreased at both low and high temperatures relative to the sedimentation coefficient obtained at 25 °C, an observation that is consistent with a smaller assembly state at both extremes of temperature.

It is well documented that ClpA forms hexamers upon nucleotide binding (*14*, *20*). A plausible model would involve a distribution of monomers, dimers, and tetramers in the absence of nucleotide interacting to form hexamers upon addition of nucleotide. Here we have shown that all of our experimental results can be modeled by a monomer−dimer−tetramer equilibrium when combined with an appropriate description of the temperature dependence of the two equilibrium constants. Because equilibrium constants will always depend upon temperature, a single self-association model with the appropriate temperature-dependent equilibrium constants appears to be the most likely explanation for these experimental observations.

The observation that the self-association equilibrium can be described by a monomer−dimer−tetramer equilibrium as a function of temperature reconciles our results with the previous examination performed by Maurizi and co-workers (*19*, *20*). In their study, they performed sedimentation equilibrium at 4 °C at two concentrations of ClpA (2.4 and 6 μM monomer) at one rotor speed of 7000 rpm and concluded that ClpA resides in a monomer−dimer equilibrium. Our sedimentation equilibrium experiments performed at ~4 °C were well described by a monomer−dimer−tetramer equilibrium. However, our experiments were performed at six ClpA concentrations from 4 to 22 μM and three rotor speeds of 12000, 15000, and 18000 rpm.

Because of the higher ClpA concentration used in our experiments, we more fully populated the tetrameric state. Thus, we conclude that, in their study, they most likely did not significantly populate the tetrameric state at the two relatively low concentration of ClpA based on the equilibrium constants measured here. Therefore, they were able to model their two sedimentation profiles with a monomer−dimer model.

A monomer−dimer−-tetramer equilibrium appears to be a more likely starting point by which ClpA would assemble into active hexamers in the presence of nucleoside di- and triphosphates. We favor this model because the presence of dimers and tetramers of ClpA in solution in the absence of a nucleotide would provide the building blocks necessary for the formation of an active hexamer of ClpA upon addition of cofactor. A monomer−dimer−tetramer equilibrium eliminates the cognitive difficulties that arise in the formation of a hexamer from a distribution of only monomers and tetramers or through the joining of two tetramers and subsequent expulsion of a dimer or two monomers of ClpA en route to formation of a hexamer of ClpA.

Temperature Dependence of the Equilibrium Constant. The tetramerization equilibrium constant displays a negative heat capacity change, $\Delta C_p^\circ = -2.03 \pm 0.35$ kcal K^{-1} (mol of tetramer)$^{-1}$. Although there are many potential sources of this heat capacity change, the negative value of ΔC_p° suggests a desolvation of nonpolar surfaces along with a restriction of movement (*44*). This is consistent with formation of tetramers, as burial of nonpolar surfaces may occur during assembly. However, it is possible that some component of this heat capacity change is from other temperature-dependent equilibria that are coupled to tetramer formation (*21*, *45*).

We were able to measure the dimerization equilibrium constant, $L_{2,0}$, at two temperatures (3.9 and 38.2 °C). With only two measured values, it is impossible to fully describe the temperature dependence of $L_{2,0}$. Multiple possibilities still exist for how the dimerization equilibrium constant may depend on temperature. However, some constraints can be made on the basis of the observation that $L_{2,0}$ can be measured at the two extremes of temperature. First, the van't Hoff plot for $L_{2,0}$ could be linear with a very slight enthalpy change. Alternatively, the van't Hoff plot could be nonlinear and concave up, thus resulting in a positive ΔC_p°. Both of these possibilities would result in the magnitude of $L_{4,0}$ being closest to the value of $L_{2,0}$ at the two extremes of temperature because of the concave down shape of the dependence of $L_{4,0}$ on inverse temperature (see Figure 6). Therefore, as the two equilibrium constants approach one another, they begin to be observed in the NLLS fitting because of the increased population of dimers and decreased population of tetramers. On this basis, it seems less likely that $L_{2,0}$ would exhibit a concave down nonlinear van't Hoff plot because, if this were the case, $L_{2,0}$ and $L_{4,0}$ would be simultaneously observed over a broader range of temperatures.

The ClpA monomer contains two nucleotide binding and hydrolysis sites. One of these sites has been shown to be involved in driving the formation of the hexamer active in polypeptide translocation (*15*). Despite this, little is known about the relative affinities of the two nucleotide binding sites, the cooperativity between the two binding sites, if any, or even if both sites are saturated on every monomer in the hexamer. To quantitatively address nucleotide binding, one must know the range of concentrations over which different assembly states are populated and what oligomeric states exist (*18*). That is to say, one must have an accurate description of the self-association equilibrium in the absence of a nucleotide. Here we have presented a detailed examination of the assembly state of ClpA as a function of both ClpA concentration and temperature. The data presented here and in our previous study are all described well by a monomer−dimer−tetramer model (*19*). With this model in hand, we are now poised to begin a quantitative examination of the energetics of nucleotide binding, the coupling to hexamer formation, and subsequent polypeptide substrate binding.

ACKNOWLEDGMENT

We thank Dr. Peter Prevelige and The University of Alabama at Birmingham Department of Microbiology for use of the Beckman XL-A analytical ultracentrifuge. We also thank Dr. Prevelige for discussion throughout this research.

REFERENCES

1. Sauer, R. T., Bolon, D. N., Burton, B. M., Burton, R. E., Flynn, J. M., Grant, R. A., Hersch, G. L., Joshi, S. A., Kenniston, J. A., Levchenko, I., Neher, S. B., Oakes, E. S., Siddiqui, S. M., Wah, D. A., and Baker, T. A. (2004) Sculpting the proteome with AAA(+) proteases and disassembly machines. *Cell 119*, 9–18.
2. Wickner, S., Maurizi, M. R., and Gottesman, S. (1999) Posttranslational quality control: Folding, refolding, and degrading proteins. *Science 286*, 1888–1893.
3. Gottesman, S. (1996) Proteases and their targets in *Escherichia coli*. *Annu. Rev. Genet. 30*, 465–506.
4. Goldberg, A. L., and St John, A. C. (1976) Intracellular protein degradation in mammalian and bacterial cells. *Annu. Rev. Biochem. 45* (Part 2), 747–803.
5. Hwang, B. J., Woo, K. M., Goldberg, A. L., and Chung, C. H. (1988) Protease Ti, a new ATP-dependent protease in *Escherichia coli*, contains protein-activated ATPase and proteolytic functions in distinct subunits. *J. Biol. Chem. 263*, 8727–8734.
6. Katayama, Y., Gottesman, S., Pumphrey, J., Rudikoff, S., Clark, W. P., and Maurizi, M. R. (1988) The two-component, ATP-dependent Clp protease of *Escherichia coli*. Purification, cloning, and mutational analysis of the ATP-binding component. *J. Biol. Chem. 263*, 15226–15236.
7. Levchenko, I., Luo, L., and Baker, T. A. (1995) Disassembly of the Mu transposase tetramer by the ClpX chaperone. *Genes Dev. 9*, 2399–2408.
8. Wickner, S., Gottesman, S., Skowyra, D., Hoskins, J., McKenney, K., and Maurizi, M. R. (1994) A molecular chaperone, ClpA, functions like DnaK and DnaJ. *Proc. Natl. Acad. Sci. U.S.A. 91*, 12218–12222.
9. Hoskins, J. R., Pak, M., Maurizi, M. R., and Wickner, S. (1998) The role of the ClpA chaperone in proteolysis by ClpAP. *Proc. Natl. Acad. Sci. U.S.A. 95*, 12135–12140.
10. Neuwald, A. F., Aravind, L., Spouge, J. L., and Koonin, E. V. (1999) AAA+: A class of chaperone-like ATPases associated with the assembly, operation, and disassembly of protein complexes. *Genome Res. 9*, 27–43.
11. Tucker, P. A., and Sallai, L. (2007) The AAA+ superfamily: A myriad of motions. *Curr. Opin. Struct. Biol. 17*, 641–652.
12. Walker, J. E., Saraste, M., Runswick, M. J., and Gay, N. J. (1982) Distantly related sequences in the α- and β-subunits of ATP synthase, myosin, kinases and other ATP-requiring enzymes and a common nucleotide binding fold. *EMBO J. 1*, 945–951.
13. Gottesman, S., Squires, C., Pichersky, E., Carrington, M., Hobbs, M., Mattick, J. S., Dalrymple, B., Kuramitsu, H., Shiroza, T., and Foster, T.; et al. (1990) Conservation of the regulatory subunit for the Clp ATP-dependent protease in prokaryotes and eukaryotes. *Proc. Natl. Acad. Sci. U.S.A. 87*, 3513–3517.
14. Maurizi, M. R. (1992) Proteases and protein degradation in *Escherichia coli*. *Experientia 48*, 178–201.
15. Singh, S. K., and Maurizi, M. R. (1994) Mutational analysis demonstrates different functional roles for the two ATP-binding sites in ClpAP protease from *Escherichia coli*. *J. Biol. Chem. 269*, 29537–29545.
16. Gottesman, S., Roche, E., Zhou, Y., and Sauer, R. T. (1998) The ClpXP and ClpAP proteases degrade proteins with carboxy-terminal

peptide tails added by the SsrA-tagging system. *Genes Dev. 12*, 1338–1347.
17. Rajendar, B., and Lucius, A. L. (2010) Molecular mechanism of polypeptide translocation catalyzed by the *Escherichia coli* ClpA protein translocase. *J. Mol. Biol. 399*, 665–679.
18. Wyman, J., and Gill, S. J. (1990) Binding and linkage: Functional chemistry of biological macromolecules, University Science Books, Mill Valley, CA.
19. Veronese, P. K., Stafford, R. P., and Lucius, A. L. (2009) The *Escherichia coli* ClpA Molecular Chaperone Self-Assembles into Tetramers. *Biochemistry 48*, 9221–9233.
20. Maurizi, M. R., Singh, S. K., Thompson, M. W., Kessel, M., and Ginsburg, A. (1998) Molecular properties of ClpAP protease of *Escherichia coli*: ATP-dependent association of ClpA and clpP. *Biochemistry 37*, 7778–7786.
21. Maluf, N. K., and Lohman, T. M. (2003) Self-association equilibria of *Escherichia coli* UvrD helicase studied by analytical ultracentrifugation. *J. Mol. Biol. 325*, 889–912.
22. Tang, L. H., and Adams, E. T., Jr. (1973) Sedimentation equilibrium in reacting systems. VII. The temperature-dependent self-association of β-lactoglobulin A at pH 2.46. *Arch. Biochem. Biophys. 157*, 520–530.
23. Suprenant, K. A., and Marsh, J. C. (1987) Temperature and pH govern the self-assembly of microtubules from unfertilized sea-urchin egg extracts. *J. Cell Sci. 87* (Part 1), 71–84.
24. Herrmann, H., and Aebi, U. (1999) Intermediate filament assembly: Temperature sensitivity and polymorphism. *Cell. Mol. Life Sci. 55*, 1416–1431.
25. Takase, K., Niki, R., and Arima, S. (1980) A sedimentation equilibrium study of the temperature-dependent association of bovine β-casein. *Biochim. Biophys. Acta 622*, 1–8.
26. Yphantis, D., and Larry, J. (1999) WinMatch V0.99 for Intercomparison of Ultracentrifuge Data Files, version 0.99, National Analytical Ultracentrifugation Center, Storrs, CT.
27. Cole, J. L. (2004) Analysis of heterogeneous interactions. *Methods Enzymol. 384*, 212–232.
28. Liu, S., and Stafford, W. F., III (1995) An optical thermometer for direct measurement of cell temperature in the Beckman instruments XL-A analytical ultracentrifuge. *Anal. Biochem. 224*, 199–202.
29. Schuck, P. (1998) Sedimentation analysis of noninteracting and self-associating solutes using numerical solutions to the Lamm equation. *Biophys. J. 75*, 1503–1512.
30. Philo, J. S. (2006) Improved methods for fitting sedimentation coefficient distributions derived by time-derivative techniques. *Anal. Biochem. 354*, 238–246.
31. Philo, J. S. (2000) A method for directly fitting the time derivative of sedimentation velocity data and an alternative algorithm for calculating sedimentation coefficient distribution functions. *Anal. Biochem. 279*, 151–163.
32. Schuck, P. (2003) On the analysis of protein self-association by sedimentation velocity analytical ultracentrifugation. *Anal. Biochem. 320*, 104–124.
33. Dam, J., and Schuck, P. (2005) Sedimentation velocity analysis of heterogeneous protein-protein interactions: Sedimentation coefficient distributions c(s) and asymptotic boundary profiles from Gilbert-Jenkins theory. *Biophys. J. 89*, 651–666.
34. Cantor, C. R., and Schimmel, P. R. (1980) Techniques for the study of biological structure and function, W. H. Freeman, San Francisco.
35. Laue, T. M., Shah, B. D., Ridgeway, T. M., and Pelletier, S. L. (1992) Computer-aided interpretation of analytical sedimentation data for proteins. In Analytical Ultracentrifugation in Biochemistry and Polymer Science (Harding, S. E., Rowe, A. J., and Horton, J. C., Eds.) The Royal Society of Chemistry, Cambridge, U.K.
36. Cole, J. L. (1996) Characterization of human cytomegalovirus protease dimerization by analytical centrifugation. *Biochemistry 35*, 15601–15610.
37. Ebel, C., Eisenberg, H., and Ghirlando, R. (2000) Probing protein-sugar interactions. *Biophys. J. 78*, 385–393.
38. McMeekin, T., and Marshall, K. (1952) Specific volumes of proteins and the relationship to their amino acid contents. *Science 116*, 142–143.
39. Veazey, W. R., Hodgman, C. D., and Chemical Rubber Company (2010) Handbook of chemistry and physics, p 57, Chemical Rubber Co., Cleveland, OH.
40. Taylor, J. R. (1997) An introduction to error analysis: The study of uncertainties in physical measurements, 2nd ed., University Science Books, Sausalito, CA.
41. Correia, J. J. (2000) Analysis of weight average sedimentation velocity data. *Methods Enzymol. 321*, 81–100.
42. Boysen, R. I., Wang, Y., Keah, H. H., and Hearn, M. T. (1999) Observations on the origin of the non-linear van't Hoff behaviour of polypeptides in hydrophobic environments. *Biophys. Chem. 77*, 79–97.
43. Baldwin, R. L. (1986) Temperature dependence of the hydrophobic interaction in protein folding. *Proc. Natl. Acad. Sci. U.S.A. 83*, 8069–8072.
44. Spolar, R. S., and Record, M. T., Jr. (1994) Coupling of local folding to site-specific binding of proteins to DNA. *Science 263*, 777–784.
45. Eftink, M. R., Anusiem, A. C., and Biltonen, R. L. (1983) Enthalpy-entropy compensation and heat capacity changes for protein-ligand interactions: General thermodynamic models and data for the binding of nucleotides to ribonuclease A. *Biochemistry 22*, 3884–3896.